The Transient Analysis of Certain TEM Mode Four-Port Networks

G. F. ROSS, SENIOR MEMBER, IEEE

Abstract—This paper presents the transient analysis of certain four-port TEM mode microwave networks. Flow graph techniques are employed to determine in closed form the system function between two given ports. This representation reveals the pole-zero pattern of the component which is used to graphically obtain the amplitude spectrum (CW response).

In the time domain, the impulse response (the inverse transform of the system function) is used to determine the step modulated response of the network at its resonant frequency. This proves to be a particularly easy task for certain symmetrical networks. The flow graph technique is illustrated by analyzing three often used microwave networks (namely; the ring hybrid, the 3-dB branch line coupler, and the branch line phase shifter), and an estimate is made of their "settling times" for a step modulated input.

Experimental methods are introduced which permit an investigator to generate a 0.2 nanosecond pulse and/or a microwave step modulated source. These test functions are then used to critically evaluate the theoretical results in the laboratory.

I. Introduction

THE CONCEPTS of linear systems as they apply to lumped networks are well known. Terms such as the impulse and step response or system function of a network have well-defined meanings and their importance is understood. The terminology and concepts of linear systems as they apply to microwave networks, however, have received only limited attention. Getsinger [1], for example, studied the impulse and step response of certain transmission line networks with the aid of a computer. The purpose of this paper is to show how the fundamental notions of linear system analysis, including the use of flow graphs, can be applied to the analysis of distributed networks. This approach yields a very convenient formulation for a particular class of microwave structures which operate in the TEM mode resulting in closed form solutions.

The properties of microwave structures can be found from a solution of Maxwell's equations subject to appropriate boundary conditions. In general, these are linear partial differential equations involving the three spatial directions x, y, and z of the electric field ($\overline{E}$) or the magnetic intensity ($\overline{H}$) and time t. Certain geometrical configurations, namely "two-wire lines" or their conformal equivalent, are able to operate with $\overline{E}_z$ and $\overline{H}_z$ equal to zero (where it has been assumed that z is the direction of propagation). These are called TEM modes, and networks capable of supporting them are commonly called TEM components. From an academic viewpoint no real structure can operate strictly in this mode since the presence of resistance in the structure demands that $\overline{E}_z$ be nonzero. In practice, however, $\overline{E}_z$ may be made much smaller than the other components of $\overline{E}$ and the concept of a TEM mode is useful.

The distinguishing characteristics of TEM mode propagation are that the concepts of voltage and current can be legitimately applied and that the performance of a TEM mode component can be described by a coupled pair of linear partial differential equations involving only the two independent variables z and t.

Many commonly used TEM mode components such as four-port hybrids, directional couplers, etc., employ lengths of uniform TEM transmission lines (i.e., the inductance and capacitance/unit length are constants, independent of z) between junctions. A uniform TEM line has the following two-port system function: the amplitude spectrum is constant, independent of frequency; the phase function is linear with frequency, implying that the uniform line introduces no dispersion in the time domain. In particular, the impulse response is simply a delayed impulse.

Where TEM lines are interconnected to form junctions, the impulse response between specified ports, in general, consists of an infinite train of impulses whose areas are functions of the reflection coefficients at these junctions. In particular, where the line lengths between junctions are integral multiples of a given length the impulses are uniformly spaced and the impulsive response is given by

$$h(t) = \sum_{k=1}^{\infty} A_k \delta(t - k\tau) \tag{1}$$

where

- A_k is a function of the reflection coefficients at the junction
- $\delta(t)$ is the Dirac delta function
- τ is a time delay depending on the geometry of the network and the propagation constant of the medium.

Manuscript received April 25, 1966; revised August 2, 1966. This paper is based on a dissertation submitted by G. F. Ross under the guidance of Prof. A. Papoulis in partial fulfillment of the requirements for the Ph.D. degree in electrical engineering at Brooklyn Polytechnic Institute [17]. The work scope was later expanded under the sponsorship of the USAF Systems Command, Rome Air Development Center, New York, J. Potenza, Project Engineer, under Contract AF30(602)-3348, March 1–November 23, 1964.

The author is with the Sperry Rand Research Center, Sudbury, Mass.

When the impulse response of a linear, time invariant network consists of a train of impulses of varied weighting, the response to an input $f(t)$ may be found conveniently by appropriately weighting and delaying replicas of the input signal $f(t)$. In particular, if the impulse train is uniformly spaced $\lambda_0/2c$ seconds apart, the response to a step modulated signal of the form

$$f(t) = \sin w_0 t \cdot u(t) \tag{2}$$

where

$$w_0 = 2\pi f_0 = \frac{2\pi c}{\lambda_0}$$

can be found throughout any given half period by a simple addition. This follows since the phase difference between weighted replicas of the input signal is either zero or 180°.

In this paper, the transient responses of certain TEM components are evaluated in the time domain by exciting the network with a step-modulated signal at a carrier frequency corresponding to the nominal operating frequency of the network, and measuring their respective "settling" times. In the frequency domain, the amplitude spectrum is obtained graphically from the pole-zero pattern of the network. The pole-zero pattern is found by factoring the numerator and denominator of the system function (i.e., the inverse transform of the impulse response).

In Section II of this paper an analysis technique is presented for determining in closed form the system function of a matched four-port coupler consisting of an interconnection of three-port TEM mode junctions. The technique is illustrated in Section III where three commonly employed microwave networks are analyzed. Section IV discusses experimental methods devised for verifying the analysis technique. The results and conclusion are summarized in Section V.

II. The Analysis Technique

Flow graph techniques (as opposed to conventional matrix methods), are chosen as the primary analysis tool because 1) they afford a clear physical representation of the interaction of reflections between junctions, and 2) by application of a simple formula they permit an evaluation of the overall response or system function of the network in closed form, thus revealing the pole-zero pattern of the system. This approach is not limited to the analysis of symmetrical networks [2], but can be applied to solving more general network configurations. Previous applications of flow graph techniques have been limited to the single-frequency analysis of microwave networks [3], [4].

The flow graph representation of a given network is not unique. That is, a network may be represented by several flow graphs each having equal validity. Some graphs may, conceptually, be easier to visualize or construct. This will be demonstrated in the examples offered in Section III. A flow graph representing the interconnection of four three-port TEM mode junctions forming a four-port network is shown in Fig. 1. The output ports of the network are assumed matched to the impedance of the driving source which for convenience has been normalized to one ohm. In the discussion that follows the reference to "ports" refers to the physical network, while the reference to "nodes" refers to the topological representation of the network, namely, the flow graph. Each port in the network is represented by two nodes in the flow graph, for example, A and A'. This is required since waves traveling in a clockwise (cw) direction in the network may experience a different reflection coefficient at a port than waves entering the same port from a counterclockwise (ccw) direction. The signal flow is described as follows:

An incident (impulse) voltage entering port A is partially reflected (due to mismatch) while the two transmitted impulses travel in a cw direction toward port B and simultaneously in a ccw direction toward port D. In the graph cw signals travel along the outer square entering the unprimed nodes; ccw signals travel along the inner square entering the primed nodes. When the transmitted impulse reaches port B, for example, a fraction of the energy is reflected back to port A while the transmitted impulse continues on to port C. The impulse reflected toward port A now travels in a ccw direction and in the graph enters node A'. Part of this signal is re-reflected toward port B (in a cw direction) therefore again entering node B in the graph forming the closed loop $(BlA'k)$. The portion of the signal transmitted beyond node A' travels in a ccw direction toward node D' resulting in similar reflections between nodes A and D'. This process is continued until the transmitted signals from nodes B' and D enter nodes A' and A, respectively, and the process repeats. The values of the branch transmittances (for example, a, b, c, $\cdots$) in Fig. 1 are chosen to be the Laplace transforms of the voltage transfer coefficients between nodes. Since the impulse response of each branch is a delayed impulse, the Laplace transforms of the voltage transfer coefficients are of the form

$$a = a(p) = a'e^{-p\tau} \tag{3}$$

where a' is real and a function of the characteristic impedances of the interconnecting lines at a junction; τ depends on the length and propagation constant of the line; and $p=\sigma+jw$, the complex frequency variable. The equation at each node is simply

$$E_{\text{incident}} + E_{\text{reflected}} = E_{\text{transmitted}}. \tag{4}$$

At node A, for example (4) becomes

$$d(p) + y(p) + i(p) = a(p). \tag{5}$$

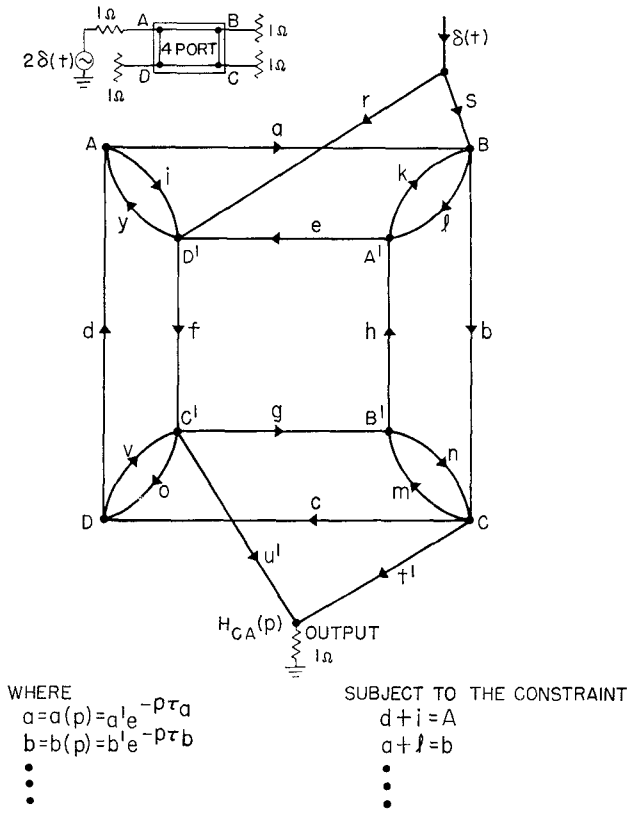

Fig. 1. Flow graph for the four-port network.

Since primed and unprimed nodes having the same letter designations, physically, represent the same port or junction in the network, special care must be exercised in introducing the excitation and taking the output from the graph. For example, if the excitation were introduced directly into the nodes (A, A'), representing the input port, two false signals would appear at the output port C. This follows since injection at these nodes would produce an initial voltage at the output port of $(ifu)+(abt)+(kbt)+(efu)$ volts as indicated in Fig. 1. From the actual network it is clear that the initial voltage must be $(abt)+(efu)$ volts. To prevent this from occurring, the input excitation weighted by the appropriate branch transmittances is introduced into the nodes which follow A, A' for both the cw and ccw waves. To obtain the output signal at port C, the outputs from both node C and C' must then be combined. Mason's formula [5], or reduction theorem, can be used to evaluate the graph. The formula states that transmission H between any two nodes in the graph is given by

$$H = \frac{\sum^{m} H_m \Delta_m}{\Delta} \tag{6}$$

where

H_m is the product of the branch transmittances of the mth forward path

$$\Delta = 1 - \sum^{n_1} L_1 + \sum^{n_2} L_2 - \sum^{n_3} L_3 + \cdots (-1)^r \sum^{n_r} L_r.$$

L_r is the product of the branch transmittances of nontouching loops taken r at a time

r is an integer

n_r is the number of closed loops

Δ_m = the value of Δ for that part of the graph not touching the mth forward path.

The use of this formula is demonstrated in the Appendix. In particular, when the line lengths between junctions are integral multiples of a given length, the system function representing the transmission from ports A to C is given by

$$H_{CA}(p) = \frac{N_{CA}(e^{-p\tau})}{D(e^{-p\tau})}, \tag{7}$$

and for the class of TEM mode components is a meromorphic function. Thus, $H_{CA}(p)$ is the ratio of two infinite polynomials in p, or

$$H_{CA}(p) = \frac{\prod_{i=1}^{\infty} (p - p_i)}{\prod_{j=1}^{\infty} (p - p_j)}. \tag{8}$$

This function can also be expressed as an infinite train of exponentials by dividing the numerator of (7) by its denominator. This result can also be obtained by taking the Laplace transform of (1),

$$H_{CA}(p) = \mathcal{L}\left[h(t) = \sum_{k=1}^{\infty} A_k \delta(t - k\tau)\right]$$

$$= \sum_{k=1}^{\infty} A_k e^{-pk\tau}. \tag{9}$$

Equating (8) and (9), one obtains

$$\frac{\prod_{i=1}^{\infty} (p - p_i)}{\prod_{j=1}^{\infty} (p - p_j)} \equiv \sum_{k=1}^{\infty} A_k e^{-pk\tau}. \tag{10}$$

It is clear from (10) that if $p = p_\alpha$ is a root of either the numerator or denominator of (7) then

$$p = p_\alpha + j\frac{2\pi}{\tau} n \tag{11}$$

is also a root, where n is an integer. Therefore, the poles and zeros of the system function are periodic in the complex p plane, and are infinitely denumerable. The introduction of the complex transformation

$$z = e^{-p\tau} \tag{12}$$

results in the periodic poles in the p plane coalescing into a finite number of poles in the z domain. The system function then becomes the ratio of two finite polynomials in z.

$$H(z = e^{-p\tau}) = \sum_{k=1}^{\infty} A_k z^k = \frac{N(z)}{D(z)} . \tag{13}$$

The transformation also maps the jw axis in the p plane onto the unit circle in the z plane; the left-half plane (LHP) maps outside the unit circle. Thus, the amplitude spectrum, defined as the magnitude of the system function, can be obtained in a conventional manner [6] by graphically evaluating $H_{CA}(z)$ on the unit circle

$$A_{CA}(\omega) = \left| H_{CA}(z) \right|_{z=e^{-j\omega\tau}}. \tag{14}$$

It should be noted that in sampled data system analysis, it is conventional to define the z transform by introducing the transformation $z=e^{+p\tau}$. This transformation maps the LHP inside the unit circle, and the poles and zeros of the system function are crowded into a confined region [7]. To increase the accuracy of the graphical evaluation the transformation given in (12) is used.

The flow graph representation offered in Fig. 1 for the four-port can be extended to include the general matched network containing an interconnection of n TEM mode three-port junctions. The graph for this configuration would consist of two concentric n sided polygons having $2n$ nodes: n nodes for cw and n nodes for ccw waves with interconnecting loops between nodes as shown in Fig. 1. For example, the topological representation for a four-port branch-line coupler of three branches consists of two concentric hexagons with two directed interconnecting loops at each node.

III. Applications

In this section the analysis technique will be illustrated by determining the transient behavior of three commonly employed microwave components; namely, the ring hybrid, the 3-dB branch line coupler, and the branch line phase shifter.

A. The Ring Hybrid

The ring hybrid is employed as a sum and differencing network in many microwave system applications [8]. In other instances it is used as a matched power divider. The ring hybrid is shown in Fig. 2(a) and is described by the normalized single frequency scattering matrix

$$S = \frac{1}{\sqrt{2}} \begin{vmatrix} 0 & 1 & 0 & 1 \\ 1 & 0 & -1 & 0 \\ 0 & -1 & 0 & 1 \\ 1 & 0 & 1 & 0 \end{vmatrix} \tag{15}$$

where

$\boldsymbol{b} = S\boldsymbol{a}$

$\boldsymbol{a}$ is the set of incident voltages

$\boldsymbol{b}$ is the set of reflected voltages.

Two in-phase signals at f_0 entering ports A and C sum coherently at port D (the sum port) and null at port B (the difference port). Equation (15) is valid only at the frequency f_0, for which the line length between junctions are $\frac{1}{4}$ or $\frac{3}{4}$ wavelengths.

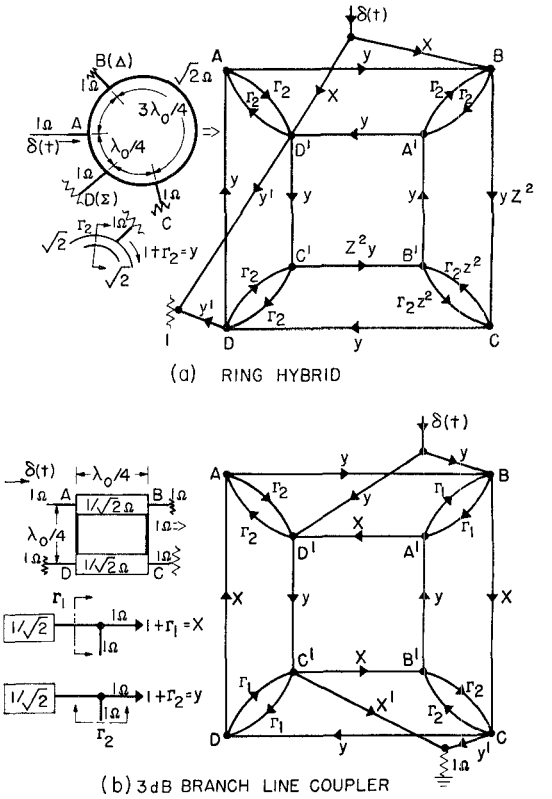

Fig. 2. Flow graph for the ring hybrid and 3-dB branch line coupler.

The flow graph for the ring hybrid [see Fig. 2(a)] is a specialized version of the graph of the four-port network shown in Fig. 1. Here, network symmetry results in many of the transmittances being equal. The transmittances of the graph are evaluated as follows.

The reflection coefficient Γ' at each junction is defined in terms of the "surge impedance" of the lines, and is given by

$$\Gamma' = \frac{Z - Z_0}{Z + Z_0} \tag{16}$$

where

Z_0 is the characteristic impedance of the driving line

Z is the terminating impedance of the line (i.e., the surge impedance of two lines in parallel

Z_0, Z are real numbers.

For example, a wave launched into the network is attenuated by the factor $x' = 1+\Gamma_1'$ where Γ_1' is defined as the reflection coefficient for a Z_0 equal one ohm line driving two $Z_0 = \sqrt{2}$ ohm lines in parallel. The transmitted cw or ccw waves leaving junctions within the network are attenuated by the factor $y' = 1+\Gamma_2'$ where Γ_2' is defined as the reflection coefficient for a $Z_0 = \sqrt{2}$ ohm line driving a one ohm and a $\sqrt{2}$ ohm line in parallel. In terms of their Laplace transforms, the branch

transmittances are given by

$$\begin{cases} x = x(p) = x'e^{-p\tau} = x'z \\ \Gamma_1 = \Gamma_1(p) = \Gamma_1'z \end{cases} \qquad \begin{cases} y = y(p) = y'e^{-p\tau} = y'z \\ \Gamma_2 = \Gamma_2(p) = \Gamma_2'z \end{cases} \tag{17}$$

where

τ is the time required for an impulse (wave) to propagate $\lambda_0/4$ meters.

$$\Gamma_1' = -\frac{2-\sqrt{2}}{2+\sqrt{2}}; \quad x' = \frac{2\sqrt{2}}{1+\sqrt{2}}$$

$$\Gamma_2' = \frac{-1}{1+\sqrt{2}}; \quad y' = \frac{\sqrt{2}}{1+\sqrt{2}}.$$

Note that four branches of the graph must contain an additional factor of z^2 (e.g., branches BC, $B'C'$, CB', and $B'C$) to account for the increased line length in these branches.

The system functions $H_{DA}(z)$ and $H_{CA}(z)$ for the ring hybrid may be found by solving the graph shown in Fig. 2(a) with the aid of Mason's formula (6). For example, the function $H_{DA}(z)$ can be evaluated with the aid of a desk calculator as shown in the Appendix where the denominator of the graph is found to be

$$D(z) = 1 - 0.5147z^2 - 0.0294z^4 - 0.412z^6 - 0.029z^8 - 0.015z^{10} + 0.00086z^{12}. \tag{18}$$

The numerator is given by

$$N_{DA}(z) = 0.485z(1 - 0.828z^2 + 0.5147z^4 - 0.5147z^6 - 0.1415z^8 - 0.032z^{10}). \tag{19}$$

In similar fashion

$$N_{BA}(z) = 0.485z(1 - 0.586z^2 + 0.272z^4 - 0.757z^6 + 0.10z^8 - 0.029z^{10}). \tag{20}$$

The formation of the graph in Fig. 1 assures that both the polynomials $N(z)$ and $D(z)$ have the common factor $(1=z^2)$. This serves as a useful check of the results since substitution of $z^2=1$ into (18) and (19) or (20) must yield 0/0. It can be seen that the error introduced by a desk calculator is small.

The impulse response is obtained by simply dividing (19) and (20) by (18) and inverting (term by term) the resulting polynomial in z. Thus,

$$h_{DA}(t) = \sum_{k=1}^{\infty} A_k \delta\left(t - (2k-1)\frac{T}{4}\right) \tag{21}$$

where

$$T = 4\tau = \frac{\lambda_0}{c}$$

$$A_1 = 0.485$$

$$A_2 = -0.153$$

$$A_3 = 0.186$$

$$\vdots$$

and

$$h_{BA}(t) = \sum_{m=1}^{\infty} \tilde{A}_m \delta\left(t - (2m-1)\frac{T}{4}\right) \tag{22}$$

where

$$\tilde{A}_1 = 0.485$$

$$\tilde{A}_2 = -0.034.$$

$$\tilde{A}_3 = 0.128$$

$$\vdots$$

These responses are plotted in Fig. 3. The step modulated response $\hat{a}(t)$ of the network at $f_0=4c/\lambda_0$ follows directly from (21) or (22). For example, consider the voltage $\hat{a}_{DA}(t)$. Assuming the first cycle of the carrier frequency is positive, it can be seen that 180° later the second term appears with a negative amplitude which is the correct polarity to add directly to the initial wave. 360° after the initiation of the step modulated signal, the third term begins with the correct phase to add coherently with the first two waves. The resonant build-up in the ring hybrid is shown in Fig. 4. The asymptotic value of the envelope of the magnitude of $\hat{a}_{DA}(t)$ is therefore

$$|\hat{a}_{DA}(t)_{\text{asymptote}}| = 0.485 + 0.153 + 0.186 - \cdots = 0.707 \text{ volts}$$

which is the single frequency value of the voltage at resonance. The envelopes of the step modulated responses at ports D and A are shown in Fig. 5. It can be seen from the figure that both responses "overshoot" their asymptotic value. There is an approximately 16 percent overshoot in the sum arm of the ring. The "settling time," or the time required for the magnitude of the envelope of the step modulated response to settle within ± 5 percent of its steady-state value is about 3 RF cycles; for example, 3 nanoseconds at 1000 Mc/s.

The roots of the system functions $H_{DA}(z)$ and $H_{CA}(z)$ can be obtained on a desk calculator using Descartes' method [9]. The results are

$$H_{DA}(z) = \frac{K_1(z^2 + 2.93 \pm j3.7)(z^2 - 0.068 \pm j1.22)}{(z^2 - 20.318)(z^2 + 1.387 \pm j4.463)(z^2 + 0.529 \pm j1.525)} \tag{23}$$

and

$$H_{BA}(z) = \frac{K_1(z^2 - 1.587 \pm j4.67)(z^2\ 0.38 \pm j1.118)}{(z^2 - 20.318)(z^2 + 1.387 \pm j4.463)(z^2 + 0.529 \pm j1.525)}. \tag{24}$$

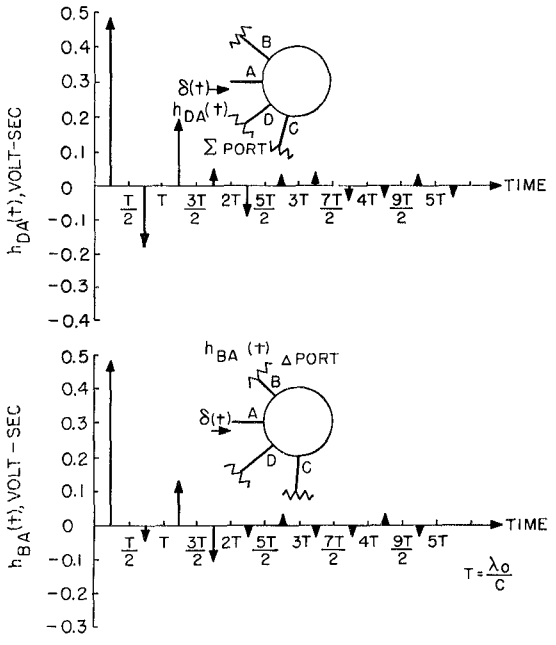

Fig. 3. Impulse response of a ring hybrid.

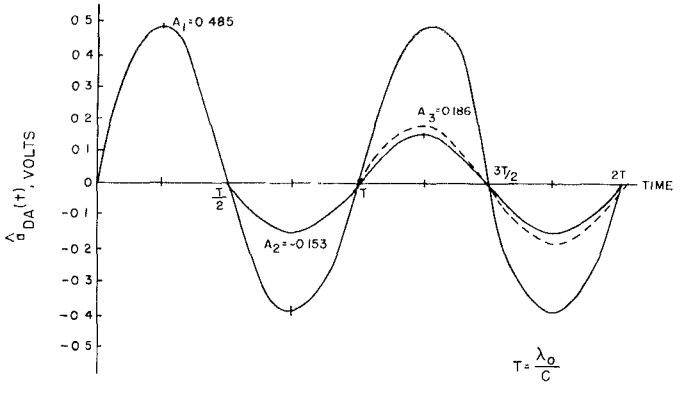

Fig. 4. The resonant buildup in a ring hybrid.

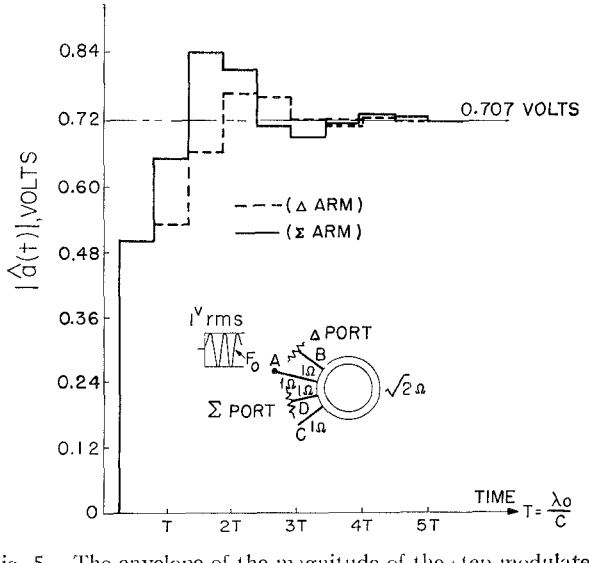

Fig. 5. The envelope of the magnitude of the step modulated response of the ring at resonance.

The poles and zeros of both system functions are plotted in Fig. 6 in the z^2 plane (where $z^2=e^{-2p\tau}$). The amplitude spectrum $A(\omega)$ is obtained graphically by forming the ratio of the product of vector magnitudes from the zeros to a point on the unit circle to the product of the poles to the same point on the unit circle. A plot of $A_{DA}(\omega)$ is shown in Fig. 7 where the output voltage at resonance has been normalized to one volt. As shown in Fig. 7, the ratio of the voltage output at resonance to that at zero frequency is equal to $\sqrt{2}$. This follows since at zero frequency the one ohm resistances from arms B, C, and D are all in parallel, and for an incident voltage of one volt the generator voltage must equal two volts; hence,

$$\frac{V\,@\,f_0}{V_{dc}}=\frac{\frac{\sqrt{2}}{2}}{2\times\frac{\frac{1}{3}}{1+\frac{1}{2}}}=\sqrt{2}. \tag{25}$$

More will be said about the utility of the pole zero diagram when the results for the branch line coupler are presented.

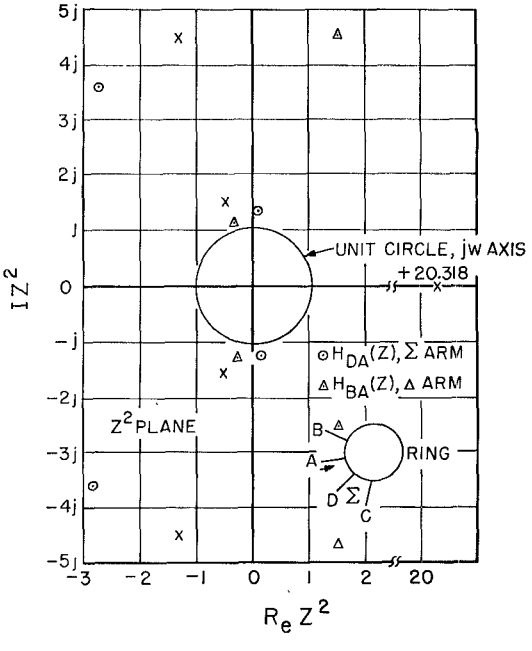

Fig. 6. Pole-zero plot for a ring hybrid.

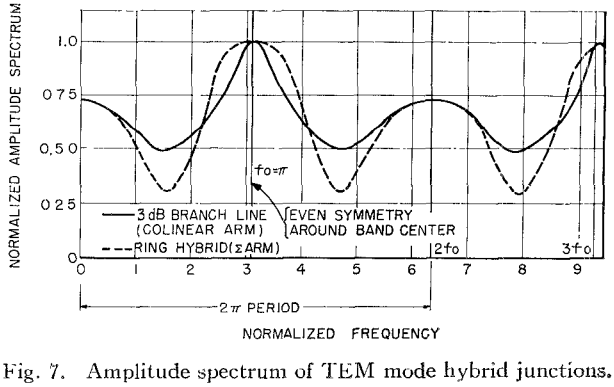

Fig. 7. Amplitude spectrum of TEM mode hybrid junctions.

B. The Branch Line Coupler

The 3-dB branch line coupler shown in Fig. 2(b) is often used as the basic building block in RF beam steering networks for electronic scanning radar systems. The hybrid phasing or Butler matrix is an example of multiple beam forming network employing 3-dB line couplers [10]. The single frequency normalized scattering matrix of the coupler is given by

$$S = \frac{1}{\sqrt{2}} \begin{vmatrix} 0 & 1 & +j \\ 1 & +j & 1 \\ +j & 1 & 0 \end{vmatrix} \tag{26}$$

and is valid at the frequency for which the line lengths between junctions are a quarter of a wavelength [11]. The flow graph for the coupler is similar to the general graph shown in Fig. 1. The symmetry of the junction in two orthogonal planes results in many of the transmittances being equal. In this graph Γ_1' is defined as the reflection coefficient for a $Z_0 = 1/\sqrt{2}$ ohm line driving two one ohm lines in parallel (that is, junctions B and D for cw waves, or junctions A and C for ccw waves). Similarly, Γ_2' is defined for a $Z_0 = 1$ ohm line driving a one ohm line in parallel with a $1/\sqrt{2}$ ohm line. The corresponding transmitted waves at each junction are

$$x' = 1 + \Gamma_1' \quad \text{and} \quad y' = 1 + \Gamma_2' \tag{27}$$

$$\begin{aligned} x &= x'e^{-p\tau} = x'z \\ \Gamma_1 &= \Gamma_1'z \\ y &= y'e^{-p\tau} = y'z \\ \Gamma_2 &= \Gamma_2'z \end{aligned} \tag{28}$$

where

τ is the time required for an impulse to propagate $\lambda_0/4$ meters

$$\Gamma_1' = -\frac{2-\sqrt{2}}{2+\sqrt{2}}; \quad x' = \frac{2\sqrt{2}}{1+\sqrt{2}}$$

$$\Gamma_2' = -\frac{\sqrt{2}}{2+\sqrt{2}}; \quad y' = \frac{2}{2+\sqrt{2}}.$$

The system functions $H_{BA}(z)$ and $H_{CA}(z)$ can be found from the graph to be

$$\begin{aligned} D(z) &= 1 - 0.402z^2 - 0.5581z^4 - 0.0688z^6 + 0.0294z^8 \\ N_{BA}(z) &= 0.485z[1 - 0.5148z^2 - 0.3135z^4 - 0.1715z^6] \\ N_{CA}(z) &= 0.485z^2[1.1716 - 0.6864z^2 - 0.485z^4] \end{aligned} \tag{29}$$

where

$$H_{BA}(z) = \frac{N_{BA}(z)}{D(z)}; \quad H_{CA}(z) = \frac{N_{CA}(z)}{D(z)}.$$

By long division one obtains

$$H_{BA}(z) = 0.485z(1 - 0.11z^2 + 0.20z^4 - 0.086z^6 + .04z^8 + \cdots)$$

and

$$H_{CA}(z) = 0.485z^2(1.17 - 0.22z^2 + 0.08z^4 - 0.006z^6 - \cdots). \tag{30}$$

The impulse response or the inverse transform of (30) is plotted in Fig. 8: the step modulated response shown in Fig. 9 follows. Once again the asymptotic value of the magnitude of the envelope of the response approaches 0.707 volts. For example,

$$\begin{aligned} |\hat{a}_{BA}(t)_{\text{asymptote}}| &= 0.485(1 + 0.11 + 0.20 + 0.08 + \cdots) \\ &= 0.707 \text{ volts.} \end{aligned} \tag{31}$$

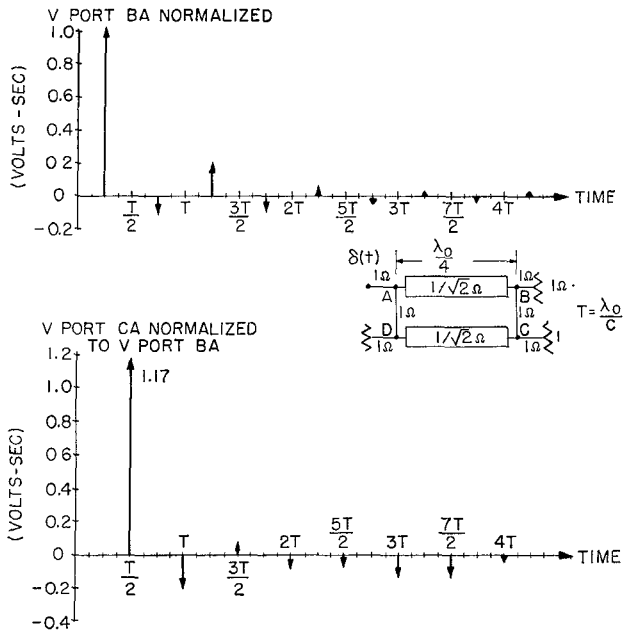

Fig. 8. Impulse response of a 3-dB branch line coupler.

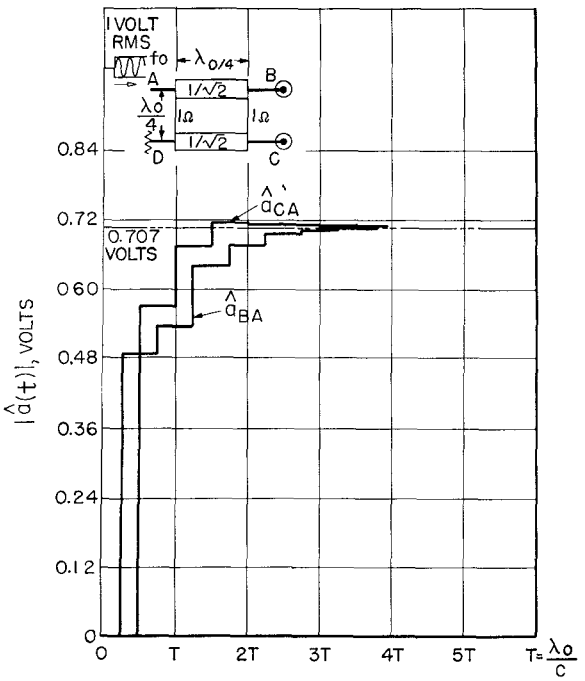

Fig. 9. The envelope of the magnitude of the step modulated response of the branch line coupler.

$|\hat{a}_{BA}(t)|$ is a monotonic increasing function with a settling time of approximately $1\frac{1}{2}$ cycles: $|\hat{a}_{CA}(t)|$ overshoots about 2 percent and has a settling time of $\frac{1}{2}$ cycle. The system functions given in (30) may be written in factored form as

$$H_{BA}(z) = \frac{C_1(z^2 + 1.41 \pm j1.96)}{(z^2 - 5.825)(z^2 + 2.245 \pm j0.893)}$$

and

$$H_{CA}(z) = \frac{C_2(z^2 + 2.31)}{(z^2 - 5.825)(z^2 + 2.245 \pm j0.893)} \quad (32)$$

where C_1 and C_2 are constants. The pole-zero diagram obtained from (32) is plotted in Fig. 10: the amplitude spectrum obtained from this diagram together with the results for the ring hybrid is shown in Fig. 6. In general, the pole zero plot is useful in describing, simultaneously, the relative behavior between networks in either the time or frequency domains. As can be seen in Fig. 10, around zero frequency the poles p_1, p_2 and zeros z_1 and z_2 act like dipoles and approximately cancel. Only pole p_3 predominates. Therefore, it is reasonable to expect the response around zero frequency to be similar to that of a simple single tuned circuit. At $z^2 = -1$ (i.e., the resonant frequency of the hybrid) it can be shown, geometrically, that this frequency is a localized maximum point of the response.

The pole-zero geometry for the ring hybrid is more complicated than that found for the branch line coupler. This might have been expected since the ring does not possess the same degree of symmetry. One pair of complex poles for the ring hybrid (see Fig. 6) is relatively close to the unit circle. This suggests that the transient behavior of the ring will be more susceptible to overshoot.

C. The Branch Line Phase Shifter

The branch line phase shifter shown in Fig. 11 is used often in microwave circuits and in antenna feed networks for array systems [12]. It employs a 3-dB branch line coupler whose output ports 2 and 3 are short circuited at a given distance L from the output reference plane. At the resonant frequency of the coupler, a 1-volt signal incident on port 1 results in a Γ volt signal into a matched load at port 4, where $|\Gamma|$ equals unity: the network is lossless. Γ is a complex number whose phase angle is a function of L. The distance L may be varied electronically by employing diodes as shown in the figure.

The 3-dB branch line coupler was analyzed in Section III-B where the transmission from ports A to B and A to C was evaluated. To analyze the phase shifter shown in Fig. 11, use will be made of the results obtained in Section III-B; however, a different flow graph technique will be employed. This is advisable since the introduction of short circuits at ports B and C introduces too many additional loops taken "r" at a time when evaluating the flow graph shown in Fig. 2(b). The flow graph will be formulated from the frequency-dependent scattering matrix of the network. That is,

$$\boldsymbol{b} = S(p)\boldsymbol{a} \quad (33)$$

where

$$\boldsymbol{b} = \begin{bmatrix} b_1 \\ b_2 \\ b_3 \\ b_4 \end{bmatrix}$$ is the set of reflected voltages at each port

$$\boldsymbol{a} = \begin{bmatrix} a_1 \\ a_2 \\ a_3 \\ a_4 \end{bmatrix}$$ is the set of incident voltages at each port.

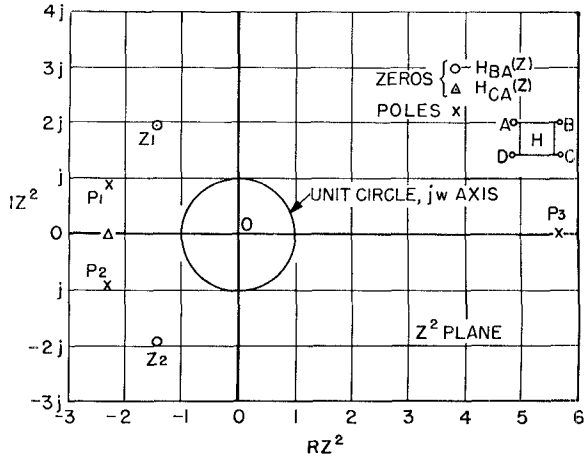

Fig. 10. Pole-zero plot for a branch line coupler.

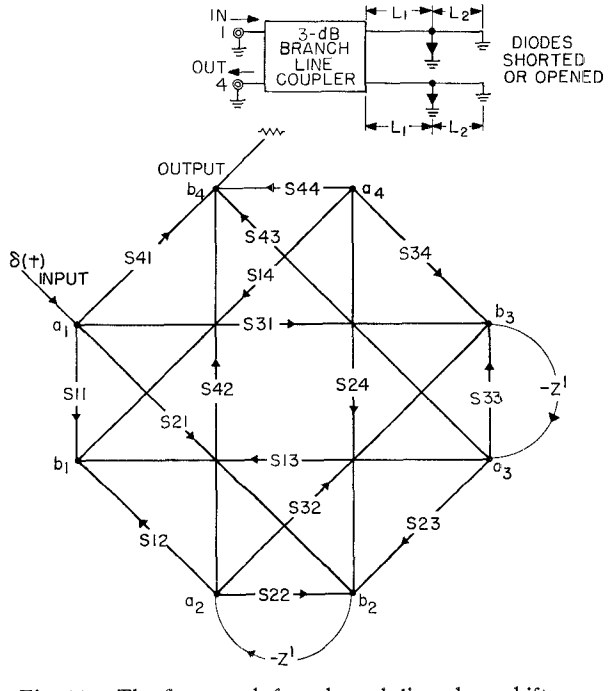

Fig. 11. The flow graph for a branch line phase shifter.

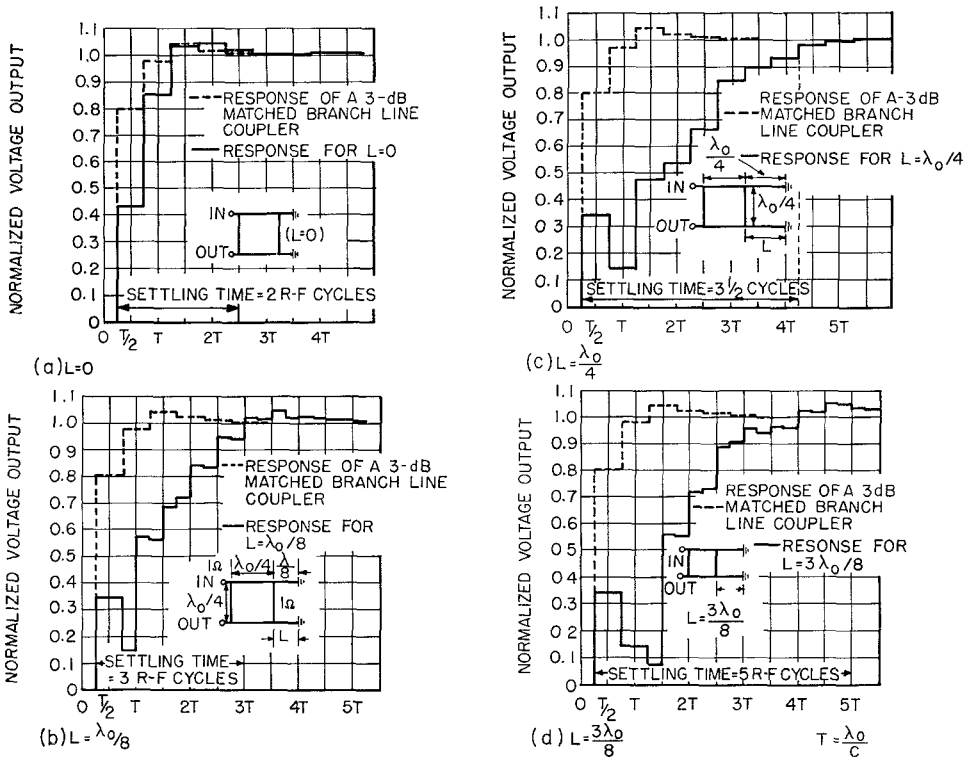

Fig. 12. Step modulated response of a hybrid phase shifter.

$S(p)$ is the 4 by 4 complex frequency scattering matrix of the 3-dB branch line coupler with matrix coefficients $S_{ij}(p)$. The ports A, B, C, and D have been relabeled 1, 2, 3, and 4, respectively, to adhere to conventional matrix notation. From the symmetrical properties of the 3-dB branch line coupler it is clear that

$$H_{CA}(p) = S_{31}(p) = S_{13}(p) = S_{24}(p) = S_{42}(p) = x$$
$$H_{BA}(p) = S_{21}(p) = S_{12}(p) = S_{43}(p) = S_{34}(p) = r \quad (34)$$

and also

$$H_{DA}(p) = S_{14}(p) = S_{41}(p) = S_{23}(p) = S_{32}(p) = y$$
$$H_{AA}(p) = S_{11}(p) = S_{22}(p) = S_{33}(p) = S_{44}(p) = s. \quad (35)$$

The transmissions $H_{DA}(p)$ and $H_{AA}(p)$ were not previously evaluated in Section III-B but are required for this analysis. They were evaluated using the flow graph of Fig. 2(b), with the proper modifications necessary for coupling into and out of the graph. After factoring out the common root of $z^2=1$ from the numerator and denominator of each transfer function, one obtains

$$x = \frac{0.5686z^2 + 0.2355z^4}{1 + 0.5980z^2 + 0.0399z^4 - 0.0289z^6}$$
$$r = \frac{0.4853z + 0.2355z^3 + 0.0833z^5}{1 + 0.5980z^2 + 0.0399z^4 - 0.0289z^6} \quad (36)$$
$$y = \frac{0.3432z + 0.4020z^3 + 0.0589z^5}{1 + 0.5980z^2 + 0.0399z^4 - 0.0289z^6}$$

and

$$s = \frac{-0.4142 - 0.4731z^2 + 0.0121z^4 + 0.0709z^6}{1 + 0.5980z^2 + 0.0399z^4 - 0.0289z^6}$$

where

$$z = e^{-pT} \quad \text{as before.}$$

As a result of the short circuits as ports 2 and 3, the output signals at these junctions are totally reflected with opposite signs and become the incident voltages a_2 and a_3, respectively.

The flow graph for the complete branch line phase shifter is thus a topological representation of (33) with the applicable boundary condition; namely,

$$a_2 = -b_2Z'$$
$$a_3 = -b_3Z' \quad (37)$$
$$Z' = e^{-p(2L/c)}$$

where L is the distance to the diode short circuit.

The flow graph of the phase shifter is also shown in Fig. 11. In terms of the graph parameters it can be shown, using (6), that

$$H_{41}(z) = y + \frac{Z'[(x^2 + r^2)yZ' - 2rx(1 + sZ')]}{1 + 2sZ' + (Z')^2(s^2 - y^2)}. \quad (38)$$

To evaluate $H_{41}(z)$, the values for x, r, y, and s given in (36), must be substituted into (38). Numerically, this is an awkward manipulation resulting in a numerator consisting of 27 terms and a denominator of 29 terms.

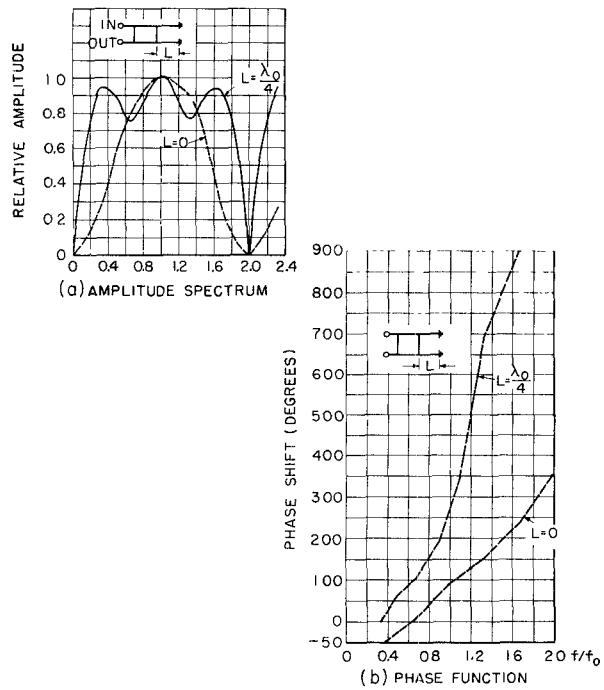

Fig. 13. The amplitude spectrum and phase function of a branch line phase shifter, $L=0$ and $L=\lambda_0/4$.

The result is of the form

$$H_{41}(z) = \frac{N(z)}{D(z)} \tag{39}$$

where

$$\begin{aligned} N_{41}(z) = {} & [0.3432z + 0.8125z^3 + \cdots + 5 \times 10^{-5}z^{17}] \\ & + Z'[-0.2844z - 1.3797z^3 + \cdots - 2 \times 10^{-4}z^{17}] \\ & + (Z')^2[0.0589z + 0.4725z^3 + \cdots 3 \times 10^{-4}z^{17}] \end{aligned}$$

and

$$\begin{aligned} D(z) = {} & [1 + 1.794z^2 + \cdots + 10^{-4}z^{18}] \\ & + Z'[-0.8284 - 1.9370z^2 + \cdots + 10^{-4}z^{18}] \\ & + (Z')^2[0.1716 + 0.3767z^2 + \cdots 10^{-4}z^{18}] \end{aligned}$$

Selecting the length L to the diode short circuit completely determines the system function $H_{41}(z)$. To evaluate the impulse response, $N(z)$ must be divided by $D(z)$ in (39). This operation was performed by a digital computer because of the numerical complexity of the expression. The resulting polynomial in z was used to determine the modulated step response of the phase shifter for $L=0$, $L=\lambda_0/8$, $L=\lambda_0/4$, and $L=3\lambda_0/8$. The results are presented in Fig. 12(a)–(d), respectively, where they are compared to the response of the matched 3-dB branch line coupler analyzed in Section III-B. It can be seen that the settling time deteriorates with increasing line length L, and approaches approximately 5 RF cycles for $L=3\lambda_0/8$; for example, 5 nanoseconds at $f_0=1000$ Mc/s.

The amplitude spectrum was not evaluated from the pole-zero pattern of (39) because of the high order of the polynomials. Instead, the digital computer was used to substitute values for the radian frequency, and the results appear in Fig. 13(a) for $L=0$, $L=\lambda_0/8$. The phase functions were also obtained and are plotted in Fig. 13(b). These nonlinearities in Fig. 13(a) and (b) suggest that the branch line phase shifter is likely to introduce considerable distortion when used to process wideband signals.

IV. Test Functions and Experimental Results

A. Test Functions

The purpose of this section is to describe the experimental techniques used to verify the theoretical results presented in the previous sections. It was shown in these sections that the impulse response of a network is a particularly important theoretical concept, but it is clear than an impulse function can neither be generated nor displayed in the laboratory. There are, however, two test functions which are of practical importance and are simply related to the impulse function. They are 1) the unit pulse of duration Δ and 2) the unit step function. For example, assume a TEM component (as described in III) is excited by a unit pulse of duration Δ, and the response $r(t)$, a "pulse train," is measured. Analytically, $r(t)$ can be found using (1) to be

$$\begin{aligned} r(t) = p\Delta(t)*h(t) &= [u(t) - u(t-\Delta)]* \sum_{k=1}^{\infty} A_k\delta(t - k\tau) \\ &= \sum_{k=1}^{\infty} A_k[u(t - k\tau) - u(t - \Delta - k\tau)] \end{aligned} \tag{40}$$

where

$$\begin{aligned} p\Delta(t) &= 1 \qquad |t| \leq \Delta \\ &= 0 \qquad |t| > \Delta \end{aligned}$$

* indicates convolution

$h(t)$ is the impulse response of the network

A_k are the unknown coefficients of the impulse response.

If $\Delta \leq \tau$ successive output pulses will not overlap and the amplitudes of pulses in the train are a direct measure of the A_k coefficients.

Often it is more convenient to generate a very fast step function as opposed to a narrow pulse. The response of a linear, time invariant network to this input is approximately the integral of the impulse response. This result can also be used, directly, to find the response to any other input by employing the Duhamel integral.

Another input which has considerable practical significance is the step modulated signal described by (2). This test signal has its principle spectral components concentrated around the nominal operating frequency

of the component: the spectrum of the unit pulse and the unit step functions have their maxima at zero frequency. Thus, the test results obtained using a step modulated function can be interpreted directly at the microwave frequencies while the other two test functions must be further manipulated, mathematically.

It was shown in the illustrative examples that the impulse response of a symmetrical TEM mode network consists of a train of impulses where each impulse is separated by one-half of the resonant RF period. For example, at $f_0=1$ GHz, this spacing equals one-half nanosecond. Thus, if the unit pulse is employed as the test source, its duration should be $\Delta<0.5\times10^{-9}$ seconds. If the test signal approximates the unit step function, its rise time should also be less than 0.5×10^{-9} seconds.

The step function can be approximated by using a tunnel diode pulser. The rise time of the resulting output signal is approximately 150 picoseconds and its magnitude is 0.25 volts. This signal is fed to the component under test and the response is displayed on a wideband sampling oscilloscope. A particularly useful instrument which can be appropriately connected to make transmission measurements of this type is the HP#1014A Reflectometer [13]. The unit contains a step function generator, a sampling oscilloscope, and appropriate synchronization and calibration circuitry. The output signal from the step generator is shown in Fig. 14(a).

The step function generated by the reflectometer can be used to generate a very short pulse with the aid of the network shown in Fig. 14(b). It can be shown that the unit step response of this network is a pulse of 1/2 volt amplitude and duration Δ, equal to $2L/c$, where L is the length of the 25 ohm stub and c is the speed of light in the medium [14]. The pulse forming network was constructed using strip line techniques. The output from this network is shown in Fig. 14(c). Note that the resulting pulse width measured at the half power points is approximately 200 picoseconds.

The stub concept can be extended to generate a step modulated signal where the buildup time of the waveform is less than 1/4 RF cycle. This generator is shown in Fig. 15(a). It consists of a cascade connection of TEM mode "T" networks similar to the one shown in Fig. 14(b). The first two stubs which are of equal length are short-circuited. Succeeding stubs are open circuited and are of increasing length. The output from the last "T" section is fed into a low-pass filter (LPF) and then to the network under test. It can be shown that the number of square cycles N generated at the output of the kth stub is given by [15]

$$N = 2^{k-2} \tag{41}$$

while the output voltage amplitude V_0 is given by

$$V_0 = 2^{-k} \text{ volts.} \tag{42}$$

The cutoff frequency of the LPF is selected to attenuate the odd harmonics (i.e., round off the corners of waveform). A 16 cycle, 1300 MHz waveform generated using this technique is shown in Fig. 15(b).

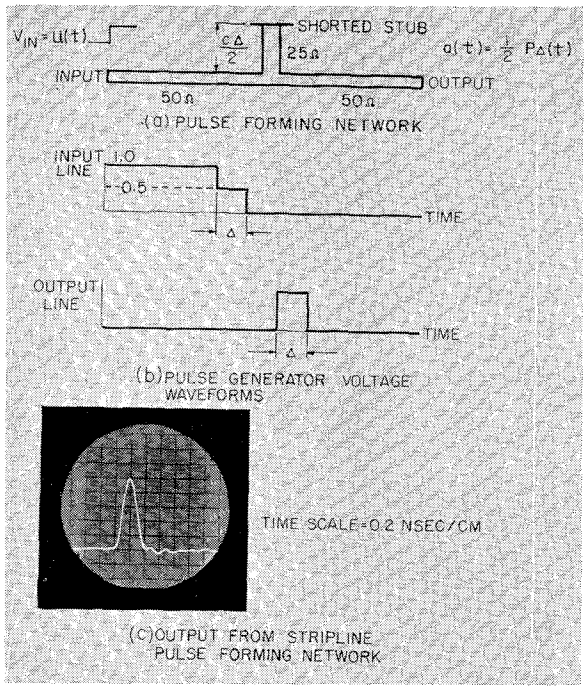

Fig. 14. 200 picosecond pulse generator.

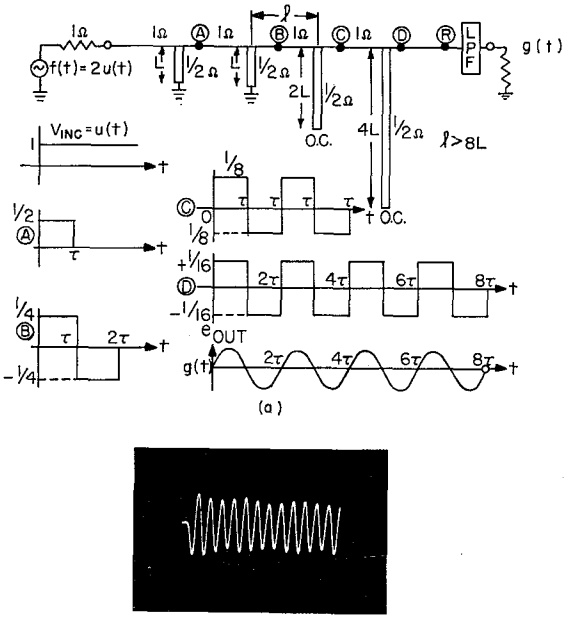

Fig. 15. The synthetic generation of a step modulated microwave source.

It should be noted that in the network shown in Fig. 15(a) there are reflections between junctions due to waves traveling in the back direction that eventually are re-reflected toward the output terminal. If the line lengths between stubs, however, are made longer than twice the length of the last stub, these undesired reflections are far removed from the trailing edge of the generated waveform.

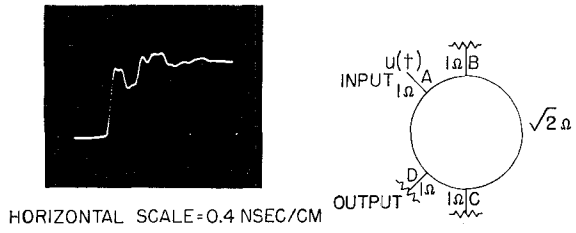

(a) PORT A TO D

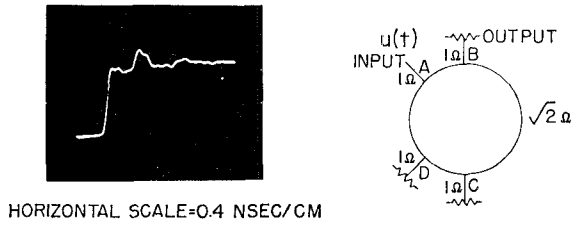

(b) PORT A TO B

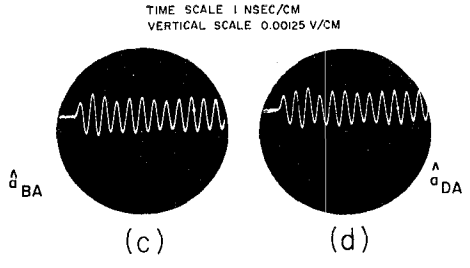

Fig. 16. The step and step modulated response @ f_0 of a ring hybrid.

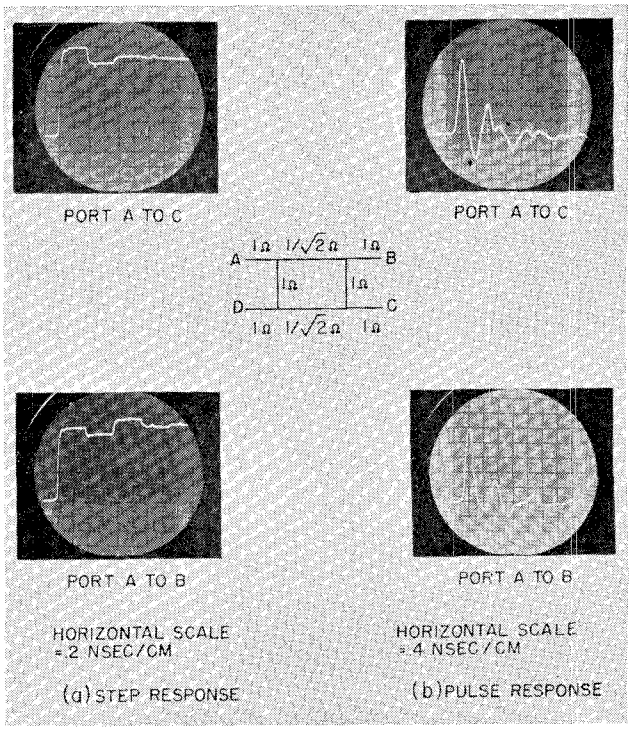

Fig. 17. The step and pulse response of a 3-dB branch line coupler.

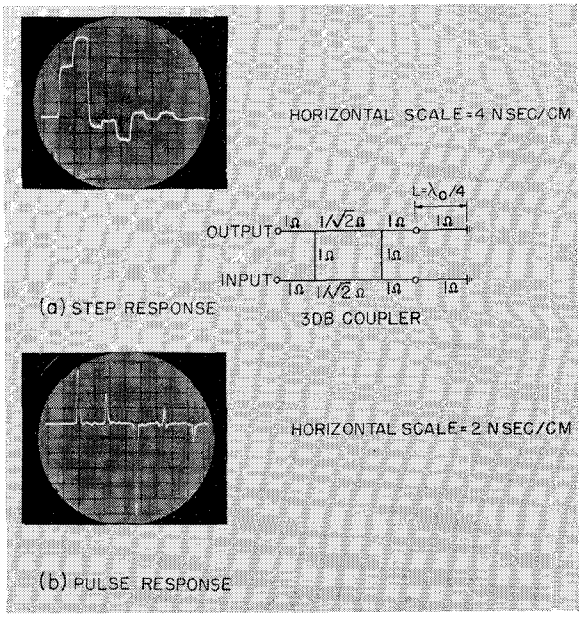

Fig. 18. The step and pulse response of a branch line phase shifter, $L=\lambda_0/4$.

B. Experimental Results

1) The Ring Hybrid: An *L*-band ring hybrid designed to operate at 1315 MHz was selected for test. The unit used a strip line construction with air as the dielectric; thus, responses are expected to be separated by 0.38 nanoseconds at the output port. The experimental results obtained using the step generator output of the HP Model 1014A reflectometer are shown in Fig. 16(a) and (b) for the transmission between the ports *A* and *D* and *B*, respectively. These results must be compared with the integral of the results already presented in Fig. 3. It can be seen that the amplitude and sign of the various steps that were obtained agree (at least qualitatively) with the theoretical results. The lack of resolution in the pictures is attributed to the finite rise time and overshoot in the step generator. When the step modulated source shown in Fig. 15 is connected to the network under test, the results [see Fig. 16(c) and (d)] agree with the responses predicted in Section III.

2) The Branch Line Coupler: The step response and the pulse response (i.e., generated by using the network shown in Fig. 14) are shown in Fig. 17(a) and (b). A 3-dB branch line coupler designed to operate at 1315 MHz was also constructed in strip line with an air dielectric having responses separated by 0.38 nanoseconds which are experimentally verified. It can be seen that the amplitude of each pulse in Fig. 17(a) and (b) are in good agreement with the results predicted in Fig. 8.

3) Branch Line Phase Shifter: To experimentally verify the theory of the branch line phase shifter extra line lengths with short circuited terminations were added at the output ports of the coupler designed to be resonant at 135 MHz. Lowering the resonant frequency of the coupler by a factor of ten significantly improves the experimental accuracy by reducing the time domain aliasing errors. The line lengths to the short circuit were adjusted to be one-quarter wavelength. The relative amplitudes of successive impulses can be obtained theoretically by dividing $N_{41}(z)$ by $D(z)$ in (39). The results are

$$H_{14}(z) = 0.343z + 0.197z^3 - 0.624z^5 + 0.0613z^7 - 0.124z^9 + \cdots. \quad (43)$$

The experimental results shown in Fig. 18 closely confirm these results. It should be noted that a discrepancy does occur in the magnitude of the 4th pulse in Fig. 18; namely, an amplitude of 0.10 volt was observed as compared to the theoretically predicted value of 0.062 volt. The discrepancy is probably due to tolerance errors in the construction of the component. The amplitude of the 4th pulse is due to the subtraction of large and almost equal reflections and hence sensitive to junction tolerances.

V. Summary

This paper has presented a technique for analyzing the transient behavior of certain four port TEM mode networks by revealing the system function in closed form. Although the examples presented in Section III concentrated on symmetrical networks it is clear that the technique presented applies equally well to unsymmetrical network configurations.

It was shown how the inverse transform of the system function (i.e., impulse response) of a TEM mode network was a very useful concept since the response to any other input could be expressed as an appropriately weighted and displaced replica of the input. In particular it was shown that the step modulated response for certain symmetrical networks at the resonant frequency was relatively simple to obtain. By factoring the system function one could obtain the pole zero plot which lead readily to a graphical evaluation of the amplitude spectrum. Further, the relative locations of the poles and zeros were used to gain physical insight regarding the transient and single frequency behavior of various devices.

Several time domain experimental techniques were introduced to help verify the theoretical results. They involved the use of the step, pulse, and step modulated functions. Since the distances between junctions in microwave networks are usually a fraction of the resonant wavelength, the testing requires a facility with fractional nanosecond pulse technology. The step modulated source proved to be a particularly useful test source since it tested the components directly at the microwave resonant frequency and did not require further mathematical manipulation.

The test sources were used to excite the three components theoretically analyzed in Section III; namely, the ring hybrid, the 3-dB branch line coupler, and the branch line phase shifter. The experimental results agreed closely with that predicted by the theory.

It was indicated how the flow graph technique could be extended to find the impulse response of a matched interconnection of n three port junctions. The graph for this network port would contain $2n$ nodes: n nodes for cw and n nodes for ccw waves and would resemble the graph shown in Fig. 1. Admittedly, the evaluation of this graph using (6) (i.e., the calculation of nontouching loops taken "r" at a time) becomes awkward.

In closing it should be noted that this paper is an abridged version of a study which included the transient analysis of other TEM components, waveguide components, cascade connections of these components, and also the analysis of a completely distributed feed network for an array system (viz., the Luneberg Lens) [16].

Appendix

Flow Graph Evaluation of the Ring Hybrid

In the appendix the evaluation of the Flow Graph representing the ring hybrid shown in Fig. 2(a) is presented. The solution to this graph for the system function $H_{DA}(z)$ is found by evaluating the individual terms in the numerator and denominator of (6). For convenience these terms are presented in tabular form. The solution is as follows, Tables I–IV.

Substituting the values of Γ_2 and y as defined in (17) into the preceding tables, and adding terms in accordance with (6) yields (after grouping similar powers of z) the denominator of the required system function,

$$D(z) = 1 - 0.5417z^2 - 0.02944z^4 - 0.4121z^6 - 0.02944z^8 - 0.01515z^{10} + 0.00086z^{12}. \quad (44)$$

The evaluation of the numerator of the system function $N_{DA}(z)$ follows in a similar manner. It can be seen that the input branch terminating on port D' produced 5 forward paths: the input branch terminating on port B produces 8 forward paths for a total of 13 forward paths. These forward paths are identified in Table V.

Grouping numerator transmittances according to similar powers of z, it follows that

$$N_{DA}(z) = 0.485z(1 - 0.828z^2 + 0.5147z^4 - 0.5147z^6 - 0.1451z^8 - 0.032z^{10}) \quad (45)$$

and finally the system function $H_{DA}(z)$ is obtained by dividing (45) by (44)

$$H_{DA}(z) = \frac{0.485(1 - 0.828z^2 + 0.51472z^4 - 0.5147z^6 - 0.1415z^8 - 0.032z^{10})}{1 - 0.5147z^2 - 0.029z^4 - 0.412z^6 - 0.029z^8 - 0.015z^{10} + 0.000866z^{12}} \cdot \quad (46)$$

TABLE I

LOOPS TAKEN ONE AT A TIME

L Taken One at a Time	Transmittance
AD'	Γ_2^2
DC'	Γ_2^2
BA'	Γ_2^2
CB'	$\Gamma_2^2 z^4$
$ABCD$	$y^4 z^2$
$A'D'C'B$	$y^4 z^2$
$ABA'D$	$y^2\Gamma_2^2$
$AD'C'D$	$y^2\Gamma_2^2$
$BCB'A'$	$y^2\Gamma_2^2 z^4$
$CDC'B'$	$y^2\Gamma_2^2 z^4$
$DABA'D'C'$	$y^4\Gamma_2^2$
$ABCB'A'D'$	$y^4\Gamma_2^2 z^4$
$BCDC'B'A'$	$y^4\Gamma_2^2 z^4$
$CDAD'C'B'$	$y^4\Gamma_2^2 z^4$
$DABCB'A'D'C'$	$y^6\Gamma_2^2 z^4$
$ABCDC'B'A'D'$	$y^6\Gamma_2^2 z^4$
$BCDAD'C'B'A'$	$y^6\Gamma_2^2 z^4$
$CDABA'D'C'B'$	$y^6\Gamma_2^2 z^4$

TABLE II

LOOPS TAKEN TWO AT A TIME

L Taken Two at a Time	Transmittance
$(AD')(BA')$	Γ_2^4
$(BA')(CB')$	$\Gamma_2^4 z^4$
$(CB')(DC')$	$\Gamma_2^4 z^4$
$(DC')(AD')$	Γ_2^4
$(AD')(B'C')$	$\Gamma_2^4 z^4$
$(BA')(C'D)$	Γ_2^4
$(ABA'D')(CDC'B')$	$y^4\Gamma_2^4 z^4$
$(DAD'C')(BCB'A')$	$y^4\Gamma_2^4 z^4$
$(ABCD)(A'D'C'B')$	$y^8 z^4$
$ABA'D'(C'D+B'C)$	$y^2\Gamma_2^2(\Gamma_2^2+\Gamma_2^2 z^4)$
$BCB'A'(AD'+C'D)$	$y^2\Gamma_2^2 z^4(2\Gamma_2^2)$
$CDC'B'(AD'+BA')$	$y^2\Gamma_2^2 z^4(2\Gamma_2^2)$
$DAD'C'(BA'+CB')$	$y^2\Gamma_2^2(\Gamma_2^2+\Gamma_2^2 y^4)$
$(ABCB'A'D')(C'D)$	$y^4 z^4\Gamma_2^4$
$(BCDC'B'A')(AD')$	$y^4 z^4\Gamma_2^4$
$(CDAD'C'B')(BA')$	$y^4 z^4\Gamma_2^4$
$(DABA'D'C')(CB')$	$y^4 z^4\Gamma_2^4$

TABLE III

LOOPS TAKEN THREE AT A TIME

Loops Taken Three at a Time	Transmittance
$(AD')(BA')(CB')$	$\Gamma_2^6 z^4$
$(BA')(CB')(DC')$	$z^4\Gamma_2^6$
$(B'C)(DC')(AD')$	$\Gamma_2^6 z^4$
$(C'D)(AD')(BA')$	Γ_2^6
$(ABA'D')(C'D)(B'C)$	$y^2\Gamma_2^6 z^4$
$(BCB'A')(AD')(C'D)$	$y^2\Gamma_2^6 z^4$
$(CDC'B')(AD')(BA')$	$y^2\Gamma_2^6 z^4$
$(DAD'C')(BA')(CB')$	$y^2\Gamma_2^6 z^4$

TABLE IV

LOOPS TAKEN FOUR AT A TIME

Loops Taken Four at a Time	Transmittance
$(AD')(BA')(CB')(DC')$	$\Gamma_2^8 z^4$

TABLE V

EVALUATION OF N_{DA}

Letter Input Node	Designation of mth Forward Path*	H_m*	Δ_m
B	BCD	$z^2 y^2$	$1-\Gamma_2^2-y^4 z^2$
	$BA'D'$	$y\Gamma_2$	$1-\Gamma_2^2-\Gamma_2^2 z^4-y^2\Gamma_2^2 z^4+\Gamma_2^4 z^4$
	$BA'D'C'D$	$y^2 z^2$	$1-\Gamma_2^2 z^4$
	$BA'D'C'B'CD$	$\Gamma_2^2 y^4 z^4$	1
	$BCB'A'D'$	$y^3\Gamma_2 z^4$	$1-\Gamma_2^2$
	$BCB'A'C'D$	$y^4\Gamma_2^2 z^4$	1
	$BCDAD'$	$y^3\Gamma_2 z^2$	1
	$BCDC'B'A'D'$	$y^6\Gamma_2 z^4$	1
D'	$D'C'D$	$y\Gamma_2$	$1-\Gamma_2^2-\Gamma_2^2 z^4-y^2\Gamma_2^2 z^4+\Gamma_2^4 z^4$
	$D'C'B'A'BCD$	$y^5 z^4\Gamma_2$	1
	$D'ABCD$	$y^3\Gamma_2 z^2$	1
	D'	1	$1-2\Gamma_2^2-\Gamma_2^2 z^4-y^4 z^2$ $-2y^2\Gamma_2^2 z^4-y^4\Gamma_2^2 z^4+\Gamma_2^4$ $+2\Gamma_2^4 z^4+2y^2\Gamma_2^4 z^4-\Gamma_2^6 z^4$
	$D'C'B'CD$	$y^3 z^4\Gamma_2$	$1-\Gamma_2^2$

* In this table each transmittance has a common factor xy' which has been factored. The value of x is also given in (17).

Acknowledgment

The author wishes to acknowledge the assistance given him by Prof. A. Papoulis, Polytechnic Institute of Brooklyn, who guided the initial study. The author also wishes to acknowledge the helpful contributions of L. Susman and J. Hanley of the Sperry Gyroscope Co., New York, during the study phase supported by the USAF.

References

[1] W. Getsinger, "Analysis of certain transmission-line networks in the time domain," *IRE Trans. on Microwave Theory and Techniques*, vol. MTT-8, pp. 301–309, May 1960.
[2] J. Reed and G. Wheeler, "A method of analysis of symmetrical four-port networks," *IRE Trans. on Microwave Theory and Techniques*, vol. MTT-4, pp. 246–252, October 1956.
[3] S. Dunn, and G. Ross, "Signal flow and scattering techniques in microwave network analysis," *Sperry Engrg. Rev.*, vol. 12, pp. 10–22, December 1959.
[4] A. Friebig, "Lineare signal fluidiagramme," *Arch. Elek. Ubertr.*, vol. 15, pp. 285–292, June 1961.
[5] S. Mason, "Feedback theory—further properties of signal flow graphs," *Proc. IRE*, vol. 44, p. 920–926, July 1956.
[6] F. Kuo, *Network Analysis and Synthesis*. New York: Wiley, 1962, p. 193.
[7] J. Truxal, *Control System Synthesis*. New York: McGraw-Hill, 1955, p. 509.
[8] G. Ross and L. Schwartzman, "Continuous beam steering and null tracking with a fixed multiple-beam antenna array system," *IEEE Trans. on Antennas and Propagation*, vol. AP-12, pp. 541–551, September 1964.
[9] H. Hall and S. Knight, *Higher Algebra*. New York: Macmillan, 1960, p. 484.
[10] J. Butler and R. Love, "Beam forming matrix simplifies the design of electronically scanned antennas," *Electronic Design*, vol. 9, pp. 170–173, April 1961.
[11] C. Montgomery, R. Dicke, and E. Purcell, *Principles of Microwave Circuits*, M.I.T. Rad. Lab. Ser., vol. 8, New York: McGraw-Hill, 1947, p. 308.
[12] K. Mortenson, "Microwave semiconductor control devices," *Microwave J.*, vol. 7, pp. 53–61, July 1964.
[13] "Time domain reflectometry," Hewlett-Packard Company, Palo Alto, Calif., Application Note 62, 1964.
[14] G. Ross, "The synthetic generation of phase-coherent microwave signals for transient behavior measurements," *IEEE Trans. on Microwave Theory and Techniques*, vol. MTT-13, pp. 704–706, September 1965.
[15] G. Ross, L. Susman, and J. Hanley, "Transient behavior of large arrays," Rome Air Development Center, New York, Tech. Rept. RADC-TR-64-581, USAF Contract AF30(602)-3348, June 1965.
[16] G. Ross, "The transient analysis of multiple beam feed networks for array systems," Ph.D. dissertation, Polytechnic Institute of Brooklyn, Brooklyn, N. Y., 1963.

Slit-Coupled Strip Transmission Lines

S. YAMAMOTO, STUDENT MEMBER, IEEE, T. AZAKAMI, MEMBER, IEEE, AND K. ITAKURA

Abstract—Two types of slit-coupled strip-line configuration are presented which are especially useful for the realization of multisection components using printed-circuit techniques. The slit-coupled configurations described consist of a pair of strips oriented face to face and either parallel or perpendicular to the outer ground planes. Coupling is achieved through a longitudinal slit. Exact conformal mapping solutions of the even- and odd-mode characteristic impedances are arranged in the forms of the design equations for both parallel and perpendicular cases. In order to facilitate design, nomograms are presented for the parallel case which give the physical line dimensions in terms of the even- and odd-mode characteristic impedances. Furthermore, the exact design equations for both parallel and perpendicular broadside-coupled strip configurations, which are considered to be special cases of the slit-coupled configurations, are presented. Formulas for the terminating lines are also included. The proposed parallel-coupled strip transmission line configurations permit smooth variation of coupling and applications to a wide variety of circuit components.

Manuscript received May 2, 1966; revised August 4, 1966.

S. Yamamoto and K. Itakura are with the Department of Electrical Communication Engineering, School of Engineering, Osaka University, Osaka, Japan.

T. Azakami is with the Nara Technical College, Nara, Japan. He was formerly with the Dept. of Electrical Communication Engineering, School of Engineering, Osaka University.

Introduction

A NUMBER of approaches to the distributed coupling effect between parallel conductors have been proposed, and applications have been made to the various circuit components, such as filters [1]–[4], directional couplers [5]–[9], channel separation filters [10]–[12], phase shifters [13], delay equalizers [14], [15], and hybrid circuits [16]–[18]. Most of these components make use of multisection-coupled transmission lines in order to provide the desired circuit performances over a wide frequency range. Typical configurations of the coupled transmission line multisection components are illustrated in Fig. 1. Combinations of these connecting types are also employed. Usually the canonical coupled sections to be connected have different coupling characteristics and close coupling is required in many practical cases.

Simple coupled strip-line configurations of the close coupling type, applicable to printed-circuit constructions, are the broadside-coupled configurations [19] shown in Fig. 2(a) for the parallel case, and in Fig. 2(b) for the perpendicular case. While design equations are available [19], [20], they are not suited to the realiza-